RSC Advances

ROYAL SOCIETY OF CHEMISTRY

www.rsc.org/advances

Modelling and optimization of critical parameters by hybrid RSM-GA for the separation of BSA using tubular configured MFI-type zeolite microfiltration membrane

R. Vinoth Kumar[1], I. Ganesh Moorthy[2] and G. Pugazhenthi[1*]

[1*]Department of Chemical Engineering, Indian Institute of Technology Guwahati, Guwahati 781039, Assam, India.

[2]Department of Biotechnology, Kamaraj College of Engineering and Technology, Virudhunagar 626001, Tamil Nadu, India.

* To whom correspondence should be addressed. Telephone: 91-361-2582264, Fax: 91 361-2582291. Email: pugal@iitg.ernet.in

Abstract

This paper deals with the fabrication of MFI-type zeolite membrane via an in-situ hydrothermal synthesis technique on low cost porous tubular ceramic substrate. To formulate the zeolite layer on the porous substrate, the hydrothermal solution was prepared using silicate solutions. The MFI zeolite (as synthesized and calcined) was characterized by X-ray diffraction (XRD), thermogravimetric (TG) and fourier transform infrared spectroscopy (FTIR) analysis. The fabricated ceramic substrate as well as zeolite membrane was characterized by field emission scanning electron microscopy (FESEM), porosity and water permeability measurement. The porosity, mean pore size and water permeability of the zeolilte membrane were evaluated to be 51%, 0.272 μm and 4.43×10^{-7} $m^3/m^2s.kPa$, respectively. The separation efficiency of the membrane in terms of permeate flux and rejection was studied with BSA as a model protein. Three operating parameters such as, BSA concentration (100-500 ppm), pH (2-4) and applied pressure (68.94-275.79 kPa) were optimized for the better separation efficiency of the membrane using response surface methodology (RSM) followed by bi-objective genetic algorithm (GA). The non-linear models predicted by RSM were further optimized by GA. The appropriate optimum conditions were obtained as BSA concentration of 100 ppm, solution pH of 2 and applied pressure of 275.79 kPa. These predicted conditions were experimentally validated and a higher permeate flux and rejection of BSA were obtained as 4.63×10^{-5} m s^{-1} and 81.98%, respectively. Further, the separation efficiency of prepared membrane was compared with other membranes used for the BSA separation stated in literature.

Key words: MFI membrane, tubular membrane, BSA separation, response surface methodology, genetic algorithm.

1. Introduction

Bovine serum albumin (BSA) has abundant biochemical applications comprising immunoblots, Enzyme-Linked-Immunosorbent Assay (ELISAs) and immunohistochemistry. It is also used as a nutrient in microbial and cell culture. In addition, it is utilized in numerous biochemical reactions, because of its low cost and stability to increase a signal in assays. BSA is a single-chain globular protein has a prolate ellipsoidal shape with 66.7 kDa of molecular weight. The dimensions of the BSA is found to be $140 \times 40 \times 40$ Å.[1] The downstream processing of BSA is a real bottleneck in biotechnological industries because of its size and shape. Nevertheless, the separation of BSA can be accomplished by changing the solution pH, because it is a charged molecule.[2] Chromatographic techniques, such as affinity chromatography and reverse-phase HPLC are widely used in industries in order to isolate ultra-pure protein.[1]

Membrane techniques such as microfiltration (MF) and ultrafiltration (UF) with polymeric and ceramic membranes have been used for protein recovery in industries. In recent years, ceramic MF membrane has received great attention by researchers for the separation of biomolecules.[3] In addition, ceramic MF membranes can be considered as an alternative for chromatographic technique, because of their high efficiency, better chemical and thermal stability, excellent anti-fouling properties, good mechanical strength and readily scalable from the laboratory to industrial settings. These membranes are made up of inorganic oxides and have better tolerance to the wide range of pH. Owing to the very high cost of the commercially available ceramic membrane, a large scale industrial application is restricted.[4] The production of ceramic membrane with low-cost materials might overcome this problem. Monash et al.[2] fabricated the γ-Al_2O_3 ceramic composite membrane for BSA separation on low cost porous support. The prepared membrane was exhibited excellent rejection of BSA (95%). Also, some

attempts were made for the fabrication of a low cost membrane using Tunisian clay, [5, 6] kaolin, [7] and Algerian clay.[8]

Zeolites are crystalline aluminosilicate inorganic materials with unique intrinsic properties such as high surface area, excellent thermal/hydrothermal stability, high shape-selectivity and superior ion-exchange ability, which form the basis for their traditional applications in catalysis and separation of small molecules.[9] Therefore, zeolites are expected to be novel chromatographic carriers for biomolecule separation. The MFI-type zeolites possess an appropriate channel structure with low siliceous in nature. Hence, these can be used as a potential applicant in removing diverse materials. It is well known that the separation of solutes by ultrafiltration (UF) and microfiltration (MF) are not only based on the pore size, but also depend on other factors such as surface charge of the membrane and electrostatic interactions between membrane and charged solutes.[2] This means that the interaction between membrane and protein as well as protein and protein can significantly affect the performance of the UF/MF membranes.[2] For the UF/MF of protein, the rejection is based on the chemical nature of the membrane, physico-chemical properties of solute and importantly electrostatic interactions between membrane and protein. It is noteworthy to mention that, the electrostatic repulsion and attraction between the protein and membrane is based on ionic strength and solution pH. Several attempts were made to study the ionic strength and pH influence on the separation of single and mixture of proteins through inorganic membranes.[10-12] Besides, the addition of NaCl enhanced the separation of protein in some extent.[3] The BSA adsorption rate on the Al_2O_3 membrane with varying solution pH was studied by Bowen and Hughes.[13] The maximum adsorption rate was observed at the isoelectric point (pI) of BSA (pI of BSA is 4.9). The BSA transmission was

found to be more with the zirconia membrane at pH 7.[14] The best rejection of BSA was obtained at lower pH.[15]

All the previously published literature on BSA separation was based on the conventional one-factor-at-a-time (OFAT) approach. The main drawback of OFAT approach is laborious, time consuming, and did not address the interaction effects on the response. In order to overcome this drawback, effective multivariate statistical technique viz., Response surface methodology (RSM) could be used. RSM has been applied successfully in several biological, chemical processes, etc. Yi et al.[16] applied RSM for the removal of oil/water emulsion from aqueous solution using the UF membrane. RSM experimental design was also applied for the removal of copper from aqueous solution using the UF membrane.[17] Besides, other stochastical optimization approaches such as artificial neural network (ANN) and genetic algorithm (GA) have also proven an efficient tool for modelling and optimization of the process.[18]

With these backgrounds, the present study focuses on the separation of BSA using tubular configured MFI-type zeolite microfiltration membrane with a cross-flow mode of operation. Tubular configuration is well suitable for handling a large volume of feeds and high flow rates, and it can be cleaned easily. Therefore, it is our intent to fabricate MFI type zeolite membrane via an in-situ hydrothermal synthesis technique on low cost porous tubular ceramic substrate. The separation efficiency of membrane in terms of permeate flux and rejection was studied with BSA as a model protein. The effects of process variables such as solution pH, concentration of protein and applied pressure on the permeate flux and percentage rejection were studied through a hybrid RSM-GA based optimization approach. To the best of our knowledge, this is the first report on the modelling and optimization by hybrid RSM-GA for the separation of BSA using a low cost tubular ceramic supported zeolite membrane.

2. Materials and methods

2.1. Materials

The starting materials utilized for the elaboration of the membrane substrate (kaolin, quartz, ball clay, pyrophyllite, and feldspar) was of mineral grade and obtained in the vicinity (Kanpur, India). Sodium hydroxide, hydrochloric acid, sodium dodecyl sulfate and calcium carbonate were purchased from Merck (I) Ltd, Mumbai. Fumed silica was acquired from Central Drug House (P) Ltd., Mumbai. Tetrapropylammonium hydroxide (TPAOH) and bovine albumin fraction V (powder) were obtained from Loba Chemie laboratory reagents & fine chemicals, Mumbai.

2.2. Preparation of MFI-type zeolite membrane on low cost substrate

The protocol adopted to elaborate the porous tubular ceramic substrate was reported in our earlier publication.[4] The tubular substrate was fabricated from locally available low cost clay materials, namely, kaolin, quartz, ball clay, pyrophyllite, feldspar and calcium carbonate by the extrusion method. The clay mixtures were mixed with the calculated amount of Millipore water to make the paste for extrusion. The obtained paste was extruded to form tubular substrate with the following characteristics: length of 100 mm, external diameter of 11.5 mm and internal diameter of 5.5 mm. The acquired tubular substrate was subjected to natural drying at room temperature (~25^{o}C) for 12 h. After which, the substrate was dried at 100^{o}C for 12 h and 200^{o}C for 12 h in a hot air oven. Subsequently, the substrate was taken to the sintering process at a heating rate of 2^{o}C/min and sintered at 950^{o}C for 6 h in a box furnace.

MFI type zeolite was used as a coating material for the membrane layer. It was prepared by a hydrothermal technique reported by Wegner et al.[19] as follows: To prepare the hydrothermal solution, 2.8 g of sodium hydroxide was dissolved in 200 ml of 1 M tetrapropylammonium

hydroxide solution in a glass beaker. Then 40 g of fumed silica was added to the solution at 90 ^{o}C under strong stirring conditions. After which, the solution was stirred for overnight and then 6.4 ml of Millipore water was added to obtain the desired composition of the gel mixture of $100SiO_2$:$5(TPA)_2O$:$5.3Na_2O$:$1420H_2O$. Then, the prepared hydrothermal solution was poured into a Teflon coated stainless steel autoclave reactor having a capacity of 300 mL. The above prepared tubular ceramic substrate was vertically positioned in the reactor. The tightly closed reactor was subjected to in-situ hydrothermal treatment for 4 h at 185^{o}C in a hot air oven. After treatment, the membrane was extensively washed using Millipore water and dried at 40^{o}C for 72 h. To eliminate the structure directing agent/template (TPA) from the zeolite channels, the membrane was calcined at 400^{o}C for 5 h in an air atmosphere at heating rate of 0.5 ^{o}C/min.

2.3. Characterization

Different techniques were used to investigate the properties of zeolite powder (as synthesized and calcined), ceramic substrate and zeolite membrane. The structure of MFI zeolite was determined by X-ray diffraction (XRD) using a Bruker A8 advance instrument working with Cu Kα radiation sources (λ = 1.54056 Å). The profiles were recorded in the 2θ ranges of 2 to 50° with a scan rate of 0.05°/s. The thermal behavior of the MFI zeolite powder was studied by Thermogravimetric analysis (TGA) using Mettler Toledo TGA/SDTA 851® instrument in an air atmosphere from 30 to 800 °C with a heating rate of 10°C/min. The FTIR spectra of MFI zeolite powder (as-synthesized and calcined) were measured in the range of 4000 to 450 cm^{-1} with KBr powder in a Shimadzu IR Affinity-1 model spectrometer. The morphological investigations of the membrane were carried out with a field emission scanning electron microscope (FESEM, JEOL JSM-5600LV). A small size of the sample was fixed on top of the stub and layered with

gold using an auto fine coating instrument (JEOL JFC-1300) preceding to morphology assessment. The porosity of the membrane is measured using the below expression: [20]

$$\text{Porosity}\,\% = \frac{W_{wet} - W_{dry}}{\rho_{water} \times V_{membrane}} \times 100 \qquad (1)$$

where, W_{wet}, W_{dry} are wet and dry weight of the membrane (dried at 120 ^{o}C for 3 h), respectively. $V_{membrane}$ is the total volume of the membrane and ρ_{water} is the density of the water. In order to estimate the wet weight of the membrane, the membrane was soaked in water for 24 h. Then, the wet weight was measured after wiping the entire water from the membrane surface with tissue paper. Five measurements were conducted for each samples and the average value was reported.

2.4. Water flux measurement and BSA separation

An in-house made cross flow filtration system was employed for the water flux measurement and separation experiments in a cross flow manner (see Figure.1). The system consists of feed tank, pump, membrane module, pressure gauge and 3 numbers of flow control valves placed at inlet, by-pass and retentate flow paths. In order to determine the water flux, the collection of permeates was measured at different applied pressures as function of time at a fixed cross flow rate. After attaining stable flux, water flux was evaluated at diverse pressures (68.94-344.73 kPa) at a preset cross flow rate (1.11×10^{-6} m^3/s) for 15 min according to the following relation:

$$J_W\,[\text{flux}] = \frac{Q\,[\text{volume of water permeated, m}^3]}{A\,[\text{area, m}^2] \times t\,[\text{time, s}]} \qquad (2)$$

Microfiltration of BSA experiments was carried out at room temperature with the same setup depicted in Figure 1. Various concentrations of BSA solution (100-500 ppm) were

prepared with Millipore water. In order to prevent the foam formation, shaking was circumvented, because, the foam can extremely interfere during the analysis of protein. Hence, the solutions were taken for analysis only after the natural dissipation of foam occurred. BSA solutions were prepared freshly and utilized within 6 h in order to avoid the aggregation of protein. To investigate the effect of pH on the rejection and permeate flux, experiments were performed at various pH values fluctuating between 2 and 4. The pH of the solutions was adjusted with NaOH and HCl. Also, the effects of applied pressure ranging between 68.94 kPa and 275.79kPa were investigated. All the cross-flow experiments were performed using 6 L of feed solution. For each experimental run, the initial 10-20 mL of protein solution passed through the membrane was discarded in order to attain a steady flux. The separation of BSA was performed for a period of 1 h at each operating conditions. The volume of the permeate was noted for 1 h in each experimental run to evaluate the permeate flux. Aliquots were taken to measure the concentration of BSA by UV-visible spectrophotometer (Thermo Scientific, UV-2300) at a wavelength of 280 nm. The percentage rejection was calculated using the equation given below.

$$R\,[\text{rejection},(\%)] = 1 - \frac{C_p\,[\text{concentration in permeate}]}{C_f\,[\text{concentration in feed}]} \times 100 \qquad (3)$$

In order to regenerate the membrane, immediately after every experimental run, the membrane was thoroughly washed with Millipore water followed by a solution containing mixture of sodium dodecyl sulfate (SDS) (2 g L^{-1}) and NaOH (20 g L^{-1}) for 30 min. After that the membrane was again washed with Millipore water to reach neutrality. Water permeability experiment was performed to check the complete regeneration of the membrane.

2.5. Response surface methodological approach

Response surface methodology (RSM) is a statistical and systematic approach employed to estimate main effects, interaction effects and quadratic effects of the variables on the response. In the RSM, two values can be assigned to each factor *i.e.*, -1 for low values (x_{min}) and +1 for high values (x_{max}). Transformed variables -1 and +1 are called coded variables (Z) and they have no unit of measure. The centre values of all variables were coded as zero.The transformation used for coded values are as follows:

$$Z = \frac{x - [(x_{min} + x_{max})/2]}{[(x_{max} - x_{min})/2]} \quad (4)$$

Uncoded or actual values (x) can be estimated from the coded values by:

$$x = Z\frac{(x_{max} - x_{min})}{2} + \frac{(x_{max} + x_{min})}{2} \quad (5)$$

In this study, Face Centred Central Composite Design (FCCCD) was used to analyse the permeate flux and percentage rejection of BSA. Variables such as concentration of BSA in ppm, pH of the solution and applied pressure in kPa were used to find the effects on the permeate flux and rejection. Table 1 shows the variable ranges and experimental design according to FCCCD. The FCCC design consists of 20 experimental runs, which includes 8 runs in the two-level full factorial portion, 6 runs in an axial portion and 6 runs in center portion. For the pure error estimation, the center portion is repeated for 6 times. The following second-order non-linear polynomial equation was used to fit the experimental data.

$$Y = \beta_o + \sum_{i=1}^{n} \beta_i X_i + \sum_{i=1}^{n} \beta_{ii} X_i^2 + \sum_{i=1}^{n-1} \sum_{j=i+1}^{n} \beta_{ij} X_i X_j + \varepsilon \quad (6)$$

where Y is the response (permeate flux and rejection), n is the number of variables, β_0 is the

model intercept term and β_i is the linear effect term, β_{ii} is the square effect term, β_{ij} is the interaction effect term, X_i and X_j is the level of the independent variables and ε is the random error. For most of the cases, the second order model represented by Eq. (6), was adequate. The fitted models (Eq. (6)) were used to find the optimum set of operating conditions for permeate flux and rejection. In order to optimize the responses, a useful approach is Derringer's desirability function methodology.[21] This approach is frequently used to optimize multiple responses. In this approach, Y_i, the responses were converted into an individual desirability function d_i. The desirability function d_i varies over the range of 0 to 1; 0 being a completely undesirable and 1 being a completely desirable or ideal response value. The overall desirability function could be written by combining all the individual desirability as given below.

$$D = \left(\prod_{i=1}^{n} d_i \right)^{\frac{1}{n}} \qquad (7)$$

where, D is the overall desirability, d_i is the individual desirability and n is the number of response. Criteria used for individual desirability of each response are given below.

$$d = \begin{cases} 0, & y < L \\ \left(\dfrac{y - L}{U - L} \right)^r, & L \le y \le U \\ 1, & y > U \end{cases} \qquad (8)$$

where, r is a weight factor, L is the lower response and U is the higher response. The statistical analyses of the experimental data were performed using Design Expert 8.0.7.1, Stat-Ease, Inc., Minneapolis, USA. All the experiments were carried out in duplicate and average values were used for further studies.

2.6. Genetic algorithm based optimization

Genetic algorithm (GA) is a powerful global non-linear optimization tool, which can be used to find the optimum conditions of the RSM predicted model. GA can also be used in multi-objective optimization problems. In general, most of the optimization problems have many objectives to be minimized or maximized or conflicting with each other. Commonly, such problems are solved by two widely used GA approaches, such as a single composite function of all objectives through the weighted sum method and finding the Pareto optimal sets of solution. In practice, the selection of the utility functions and accurate weight functions are much difficult in the case of weighted sum approach. Hence, the Pareto optimal sets of solution approach were adopted in this present investigation, in order to find the optimal solution set. In this study, there are two objective functions, *viz,* permeate flux and percentage rejection that has to be maximized through GA. The general multi-response GA problem steps are given below.

$$x = \{x_1, x_2, \cdots x_n\} \quad (9)$$

where x is the input decision variable vector with *n*-dimension.

$$\vec{x}^{\,*} = \left[x_1^*, x_2^*, \cdots x_n^*\right]^T \quad (10)$$

where $\vec{x}^{\,*}$ is the vector, that can be obtained through the Eq. (9), which will stratify the equality and inequality constrains. Then the Eq. (10) can be used to optimize the objective function of vector, which is given below.

$$\vec{f}\left(\vec{x}\right) = \left[f_1(\vec{x}), f_2(\vec{x}) \cdots f_n(\vec{x})\right] \quad (11)$$

In this study, three input vectors such as concentration of BSA (ppm), solution pH and the applied pressure (kPa) were used. The initial populations of input vectors called chromosomes, are randomly formed. Then, according to objective functions, the input vectors fitness was evaluated. Finally, the most important genetic algorithm operations like mutation followed by

cross-over were implemented to the appropriate chromosomes to generate another set of chromosomes. This procedure continued until optimal Pareto representative subset solutions were found. In this present investigation, the models predicted by RSM were used as the objective function for multi-response GA for the maximization of permeate flux and rejection. According to the method described by Konaket al.[22] the parameters and the conditions of multi-response GA are described below.

1. Double vector population type with the population size of 20 was used.
2. To generate the initial population, the constraint dependent uniform distribution function was implemented.
3. Tournament selection function was used to choose the appropriate individual vector.
4. The reproduction crossover fraction of 0.8 was used with constrain dependent mutation function and scattered crossover function to create children for the next generation.
5. The forward direction migration option was adopted for the migration of individuals between populations. According to the forward direction migration, the individual migrates to the subsequent subpopulations.
6. Population Pareto front fraction of 0.35 was used to preserve the maximum population fit and to retain a diverse population.

The fitness function used in this study is mentioned below.

$$\max\ y_i = f(x);\ i = 1, 2 \cdots n \qquad (12)$$

where y_i represents the responses of RSM predictive models, such as permeate flux and rejection; $f(x)$ represents the non-linear quadratic model equations obtained by RSM modelling and x represents the independent vector. Equation (12) was subjected to the following criteria of lower and upper bound of input vectors.

$$
\begin{aligned}
&100 \le x_1 \le 500; && x_1 - Concentration\ of\ BSA\ in\ ppm \\
&2 \le x_2 \le 4; && x_2 - Solution\ pH \\
&68.94 \le x_3 \le 275.74; && x_3 - Applied\ pressure\ in\ kPa
\end{aligned} \qquad (13)
$$

GA multi-objective tool box of MATLAB 7.10.0 (R2010a) (The Mathworks, Inc., Natick, MA, USA) was used for the maximization of permeate flux and rejection.

2.7. Validation of optimum conditions predicted by hybrid RSM-GA

Experiments were carried out at the optimized conditions predicted by hybrid RSM-GA in duplicate in order to validate the feasibility, suitability and accuracy of the optimized conditions. The average values of the permeate flux and rejection were compared with the predicted values of RSM-GA.

3. Results and Discussion

3.1. Characterization of MFI-type zeolite

MFI-type zeolites (as-synthesized and calcined) were characterized to verify its purity and structure through XRD profile as illustrated in Figure 2. The powder XRD pattern of MFI zeolite shows the high crystallinity and the obtained profile is good agreement with patterns of MFI zeolites described elsewhere.[19] The distinctive peaks are obtained in 2θ range around 7.5 and 23.5 with some other bearing peaks in both samples signifying the occurrence of pure phase of the zeolite. The TGA and derivative thermogravimetric (DTG) curves of as-synthesized zeolite material are presented in Figure 3. The weight loss below 150^{o}C corresponds to the removal of the physically adsorbed water present in the sample and the loss at 500^{o}C is due to condensation of silanol groups. The sample exhibits a derivative peak in the range of 350-500^{o}C, which belongs to the release of structure directing agent (template) present inside the zeolite channels. The total weight loss of the zeolite is found to be 23.22%, which is mainly due to the

structure directing agent loosely occluded inside the zeolite channels, resultant in a mass loss.[23] "In Figure 4, FTIR spectrum confirms that the creation of zeolite phase in both samples presenting well defined bands around 450 cm^{-1}(T-O bending), 540 cm^{-1} (double ring vibration), 790 cm^{-1} (external symmetric stretch) and 1080 cm^{-1} (internal asymmetric stretch).[24] The external asymmetric stretching vibration near 1225 cm^{-1} occurred in the pattern of MFI structures is allocated to four chains of 5-member rings formed around a two-fold screw axis. The band appeared at 1622 cm^{-1} belongs to the bending vibration of adsorbed water. For the as-synthesized sample, the sharp intense bands occurred near 2,900 and 2,850 cm^{-1} correspond to the presence of C-H stretching of the structure directing agent (TPA). Moreover, the spectrum verifies the decrease of silanol group after calcination of zeolite at 400 ^{o}C. The bands representing 3200-3700 cm^{-1} (OH groups), also including water, as well as the band allied with silanol nests (950 cm^{-1}) evidently show a reduced intensity after calcination due to the removal of the structure directing agent (TPA).[25]"

3.2. Characterization of tubular MFI-type zeolite membrane

FESEM was used to analyze both inner and outer surface morphology of the elaborated substrate and the obtained top surface images are depicted in Figure 5 (a, b). These images provide information on consistency of prepared substrate surfaces. One can see a homogeneous surface with no cracks. Figure 5 (c, d) illustrates the FESEM images of inner and outer top surfaces of the zeolite membrane at the same magnifications. Homogeneous depositions were obtained on both sides. In a similar fashion, the figures demonstrate the homogeneous top surfaces having uniform and interconnected zeolite crystals with no observable macro-cracks. The overall morphological study concludes that the sufficient amount of zeolite crystals is loaded on the ceramic substrate surface, resulting in the formation of a compact membrane. The average

porosity of the prepared tubular ceramic substrate and MFI membrane is calculated to be 53 and 51%, respectively. Figure 6(a) illustrates the water flux of the ceramic substrate and zeolite membrane as a function of time for various applied pressures. The steady flux is attained for the entire measured time. The variations of applied pressure on water flux are also presented in Figure 6(b). It can be noticed that the water flux increases linearly with an increase in the applied pressures (68.94 - 344.73 kPa). This stipulates that the variation in the pressure is the barely driving force for permeation. For transportation operation exclusively by convection, the flow rate is proportionate to the pressure, and is in accordance with Darcy's law. The water permeability (L_h) is determined from the slope of the pure water flux (J_W) versus applied pressure across the membrane (ΔP). The water permeability (L_h) of the ceramic substrate and zeolite membrane is calculated as 5.93×10^{-7} $m^3/m^2s.kPa$ and 4.43×10^{-7} m^3/m^2s kPa, respectively. The average pore size is determined using Hagen Poiseuille expression by assuming pores are cylindrical in shape.[20]

$$J_W = \frac{\varepsilon r^2 \Delta P}{8 \mu \tau l} = L_h \Delta P \qquad (14)$$

where, ε is the porosity of the membrane, r is the pore radius of the membrane, l is the pore length, τ is the tortuosity factor, μ is the viscosity of water, L_h is water permeability and ΔP is the applied pressure. The average pore size of the ceramic substrate and zeolite membrane is calculated to be 0.309 μm and 0.272 μm, respectively. As stated above, the porosity, water permeability and mean pore size of the zeolite membrane are decreased and mass of the membrane is increased from 8.8347 g (substrate) to 9.5191 g (membrane), which is obviously due to the incorporation of the zeolite layer on the ceramic substrate by hydrothermal treatment.

3.3. Microfiltration of bovine serum albumin

The prepared tubular zeolite membrane was utilized for the separation of BSA. The concentration of BSA, initial pH of the solution and applied pressures are the important variables that affect the separation process in terms of permeate flux and rejection. Hence, the effect of these parameters was investigated.

3.4. Response surface methodological approach

To achieve a maximum permeate flux and percentage rejection of BSA, three important process parameters such as concentration of BSA, initial pH of the solution and applied pressure were considered in the cross-flow microfiltration. Initially, pH of the solution was varied from 3 to 8. It was observed from the preliminary experimental runs that the rejection is considerably very low (10-20%) beyond the isoelectric point (pI) of BSA. The pI of BSA is 4.9. At pH<pI, the charge of BSA is positive, whereas the solution pH>pI, the charge of BSA is negative. The change in solution pH will affect the electrical charge of BSA, its molecular shape and size and membrane electrical charge.[2,15] In addition, the pH of the solution will also affect the permeation flux and rejection. Based upon the preliminary experimental results, it was decided to maintain the solution pH below than that of pI of BSA. Hence, the pH of the solution altered between 2 and 4. According to the FCCCD, experiments were performed with different combinations of three independent parameters (see Table 2) in the tubular cross-flow microfiltration experimental setup. Permeate was collected for 1 h and the flux as well as BSA concentration in the permeate solution was measured. The data were fitted with a second-order polynomial equation represented by Eq. (15) and Eq. (16) for the permeate flux and percentage rejection of BSA, respectively in terms of actual values of independent variables.

$$\begin{aligned} Y_1 = {} & 4.46502\times10^{-5} - 1.31875\times10^{-7}X_1 - 7.51846\times10^{-6}X_2 - 3.5214\times10^{-8}X_3 \\ & - 5\times10^{-10}X_1X_2 + 6.76819\times10^{-11}X_1X_3 + 1.81291\times10^{-8}X_2X_3 + 1.73182\times10^{-10}X_1^2 \\ & + 1.22727\times10^{-6}X_2^2 + 2.73661\times10^{-10}X_3^2 \end{aligned} \quad (15)$$

$$Y_2 = 144.05618 - 29.992527 \times 10^{-2} X_1 - 47.9240003 \times 10^{-1} X_2 - 25.702464 \times 10^{-2} X_3 + 37.88125 \times 10^{-3} X_1 X_2 + 17.748 \times 10^{-5} X_1 X_3 + 37.64805 \times 10^{-3} X_2 X_3 + 24.497 \times 10^{-5} X_1^2 - 43.4636364 \times 10^{-1} X_2^2 + 38.971 \times 10^{-5} X_3^2 \quad (16)$$

where, Y_1 and Y_2 are permeate flux in m s^{-1} and percentage rejection of BSA, respectively.

3.5. Model adequacy checking

It is more essential to verify that the developed model gives an adequate approximation to experimental values. Optimization of the developed model will give misleading or poor results, unless otherwise the developed model shows the reasonable fit.[26] Various statistical parameters were determined to check the adequacy of the model. Besides, various diagnostic and influence plots were constructed to validate the model adequacy. They were discussed in the following section.

3.5.1. Statistical parameters for model adequacy

The statistical significance of each individual, interaction and quadratic terms in the model equations (Eq. (15) & Eq. (16)) were evaluated by the *F*-test for analysis of variance (ANOVA). Table 3, shows the quadratic models of the permeate flux and rejection of BSA for three independent variables. All the model terms are significant ($p<0.05$ at 95% confidence level), apart from the interaction terms between BSA concentration and solution pH for the response permeate flux. As shown in Table 3, the model F-value for each response (15300.27 for Y_1 and 2095.651 for Y_2) is high with a low probability value ($p<0.0001$) that reveals a high significance of the developed regression model. The F-value of lack of fit is found to be 1.624 and 0.397 respectively for the response Y_1 and Y_2 with the probability p-value greater than 0.05. This indicates that each response is not significant relative to pure error, suggesting that the predicted models correlate well with the experimental data.[27] A high determination coefficient (R^2) of each response (0.99992 for Y_1 and 0.99947 for Y_2) indicates a better correlation between

experimental and predicted values. Besides, the adjusted R^2 (0.99986 for Y_1 and 0.9989 for Y_2) and predicted R^2 (0.99935 for Y_1 and 0.99776 for Y_2) has good agreement with the determination coefficient, indicating that the aptness of the models.[28] Adequate precision measures the signal to noise ratio, in general the value greater than 4 is desirable. Adequate precision values are found to be 436.20 and 181.05 for the response Y_1 and Y_2, respectively. These high values signify that both the models could be used to navigate the design space. In addition, a relatively low value of coefficient of variation (0.48% for Y_1 and 0.71% for Y_2) suggests that experiments conducted are precise and reliable.[27,29] Absolute average deviations (AAD) between the predicted and observed data are calculated to check the accuracy of the models. AAD was calculated by the following equation:

$$AAD = \left\{ \frac{\left[\sum_{i=1}^{n} \left(\left| y_{i,\exp} - y_{i,cal} \right| / y_{i,\exp} \right) \right]}{n} \right\} \times 100 \qquad (17)$$

where, $y_{i,\exp}$ and $y_{i,cal}$ are the experimental and calculated responses, respectively, and n is the number of experimental runs. A relatively small value of AAD (0.0073% for Y_1 and 0.0042% for Y_2) displays that the model equation defines the true behaviour of the system and it could be used for interpolation in the experimental domain. Predicted error sum square (PRESS) measures how a model fits each point in the design. Generally, a small value of PRESS is desirable. PRESS values of each response are found to be 1.7034×10^{-12} and 7.0596. It implies that the predicted models are well fitted and can be used to predict the response of a new experiment. Bias is an estimator used to find out the normal distribution of errors between the experimental and predicted value. Bias can be calculated as follows:

$$Bias = \exp\left[\frac{1}{n}\sum_{i=1}^{n}\ln\frac{y_{i,\exp}}{y_{i,cal}}\right] \quad (18)$$

In this study, bias value of 1 for each response points out that errors are normally distributed, demonstrating a good model fit.

3.5.1. Diagnostic and influence plots for model adequacy

Figure 7 and 8 show diagnostic and influence plots, respectively used for model adequacy checking. Diagnostic plots were constructed based on the residues obtained. Residual or random error is the difference between the experimental and predicted value of response. Figure 7 (a-i & a-ii) show the normal probability plot of the studentized residual for the permeate flux and percentage rejection of microfiltration of BSA. From these plots, it is clearly seen that the residuals of the response are normally distributed, as they lie on very close to a straight line, which shows no deviation of variation. Figure 7 (b-i & b-ii) shows the plot of the residuals versus the ascending predicted response values. It tests the assumption of constant variance. From these plots, there is no evidence of obvious patterns established in both the responses; moreover, the plots are random scatter, indicating there is no need for a transformation. The plot of the actual response versus predicted response values is illustrated in Figure 7 (c-i & c-ii) for each response. It is clearly evident that the actual responses are relatively close to the predicted responses, and the points of all actual and predicted responses fall very close to the 45˚ line. These results indicate that the model developed are successful in confining the correlation between the process variables on the permeate flux and rejection of BSA. Figure 7 (d-i & d-ii) displays the plot of residuals versus run number. This plot is used to find the lurking variables that possibly affect the dependent variable in the course of experimentation. The data points in the plot must be scattered. From the figure, it is apparent that all data points are scattered randomly and lies within the limit (± 3). Thus, the experimental data were found satisfactory.

Figure 8(a) shows the plot of leverage versus run number. Leverage is the potential for a design point to influence the fit of the model coefficients, based on its position in the design space. Leverage equal to one indicates that there is a problem with the data point, and this unexpected error strongly influences the model. In this investigation, there is no evidence of unexpected errors and no outliers in the developed models, since the leverage value is less than 1 for both the responses (Figure 8(a-i) & (a-ii)). The variation in beta values (DFBETAS) plot (Figure 8(b)) measures the influence of each experimental run on each regression coefficient. A large DFBETAS value indicates that the particular observation has a lot of influence on the particular regression coefficient. In this study, DFBETAS plot (Figure 8(b-i) & (b-ii)) demonstrates no influence of any observation on any regression coefficients of the developed models for the permeate flux and rejection of BSA.

3.6. Effects of process variables on separation efficiency

The effect of three parameters (concentration of BSA, solution pH and applied pressure) were investigated at three levels (-1, 0 and +1) as per face centred central composite design in order to know the potential of the prepared membrane. The interaction effects of these variables on the responses are shown in Figure 9. These contour plots of response surface are plotted on the basis of a model equation to determine the interaction among the variables. These graphs are constructed by plotting against any two independent variables respectively for x and y axis with the response as a parameter, while another variable is maintained at its center (0) level.

3.6.1. Effect of concentration of BSA

The substantial decrease in permeate flux and rejection is observed with an increase in the concentration of BSA. The concentration of BSA molecules on the surface of the membrane increases with an increase in the feed concentration, which causes additional fouling resistances.

Therefore, the declination in permeate flux is observed owing to concentration polarization and partial plugging of the membrane at higher concentration. The rejection values obtained at these concentrations also demonstrate that the observed rejection decreases with increasing feed concentration. This is a typical characteristic of charged membranes, for which Donnan exclusion plays a vital role.[10,15,30] With increasing BSA concentration, the effect of Donnan exclusion declines and also the surface concentration increases, which leads to the harsh concentration polarization. Consequently, the solute permeation by diffusion increases and hence the permeate concentration also raises. The effect of each linear, interaction and square terms on the response was determined by the coefficient of estimate of each terms, which are given in the table 3. The negative sign indicated that the particular variable exhibited negative effect on the response. Similarly, the positive sign indicated that the particular term exhibited positive effect on the response. From Table 3, it is clearly seen that the coefficients of the linear term of BSA concentration exhibits negative effect on both responses. However, the quadratic term coefficients of feed concentration displays significant ($p<0.05$ at 95% confidence level) positive effect on both responses. The interaction terms except the interaction between the feed concentration and solution pH, demonstrate positive effects on permeate flux and rejection. The interaction effects of BSA concentration on responses are shown in Figure 9.

3.6.2. Effect of pH

The solution pH is the most significant physico-chemical parameter that influences the separation efficiency of microfiltration of BSA.[31] BSA separation efficiency is very low at its pI. At pI, BSA molecules possess the neutral charge. Moreover, the solubility of BSA in aqueous solution is less at pI. Below the pI, the BSA exhibits a positive charge, while above the pI, the charge of BSA is negative. Generally, the membrane surface charge is strongly dependent upon the solution pH. The point of zero charge (PZC) of MFI- type zeolite was found to be 4.[32] The

solution pH < 4, the membrane exhibits a positive charge, whereas, pH > 4, the membrane is negatively charged. In this present study, the effect of pH ranging between 2 and 4 was examined to evaluate the separation efficiency of the membrane. Hence, the charge is positive for both the BSA molecule and the fabricated zeolite membrane. A significant interaction effects are observed between the process variables as depicted in Figure 9. The coefficients of the linear term of pH show negative effect for both the responses (see Table 3). However, the interaction terms, excluding the interaction between BSA concentration and pH, display significant effects with probability, $p<0.05$. In addition, the coefficient of the quadratic effect is positive for the permeate flux and negative for the percentage rejection (Table 3). It is noteworthy to mention that, a higher rejection of 81.68% with permeate flux of 4.6×10^{-5} m s^{-1} is observed at lower pH value of 2. At the lower pH, both the membrane and BSA are positively charged, which induces the electrostatic repulsive force between BSA molecules and membrane, causing a higher rejection. The percentage rejection is found to be low (42.84-48.11%) at pH 4 (Table 2). Nevertheless, the permeate flux decreases at lower pH, and increases at pH 4. The permeate flux is strongly influenced the three process parameters. From the Figure 9, it can be shown that the strong interaction between the variables studied on the permeate flux. Perssonet al.[10] also observed a higher flux and transmission of BSA at lower pH (pH-3). Similarly, Monash et al.[2] obtained a maximum rejection of BSA (89%) at pH 3.

3.6.3. Effect of applied pressure

The permeate flux and rejection trend of BSA with various applied pressures are shown in Figure 9. The permeate flux increases with increasing applied pressure. However, the decrease in flux is observed with increasing concentration of BSA, which is mainly due to fouling. The effects of linear, interactive and square terms are given in the Table 3. It is evident from the

Table 3, that all the effects of linear, interactive and square terms are statistically significant with the probability, $p < 0.05$ at 95% confidence level. The higher permeate flux (5.54×10^{6} m s^{-1}) is obtained at 275.79 kPa. Owing to the larger driving force at higher pressure results in increased permeate flux.[20] Nonetheless, the flux of BSA solution is considerably lesser than that of pure water flux. This indicates that the presence of BSA molecules causes an additional resistance to flow.[4] The non-linear trend of rejection was observed with varying applied pressure (see Table 2). Although, the applied pressure shows a significant effect on the percentage rejection, the concentration of BSA and solution pH are predominate factors than that of applied pressure.

3.7. Prediction of optimum conditions through hybrid RSM-GA

The Derringer's desired function methodology (see section 2.5) was adopted for predicting optimum conditions for separation efficiency with maximum desirability. In this numerical optimization technique, the possible goal for the process input variables were set as in range, whereas, the goal of the responses were set as maximize with the weight factor of 1 according to the equation 8. According to this approach, optimal values were found to be as follows: BSA concentration of 100 ppm, solution pH value of 2 and applied pressure of 275.79 kPa. The maximum permeate flux and rejection were predicted as 4.594×10^{-5} m s^{-1} and 81.54%, respectively at the optimum conditions with the reasonable desirability function value of 0.830. Further, the multi-response GA was adopted as mentioned in the section 2.6, to obtain appropriate parameters for the separation efficiency. The RSM numerical optimization gives a local solution to the non-linear model, whereas, GA offers global solution.[33] Hence, GA was implemented in this study to obtain a global optimum solution of RSM predictive models. The predicted RSM models for the permeate flux and rejection were used as the fitness functions in GA. The multi-objective GA yields a set of non-inferior Pareto optimal solutions. The plot of Pareto front was drawn between two objective functions such as permeate flux and rejection and

is illustrated in Figure 10. From the Pareto front analysis, the appropriate conditions were estimated to be BSA concentration of 100 ppm, pH value of 2 and applied pressure of 275.79 kPa, at which the permeate flux of 4.69×10^{-5} m s^{-1} and 82.17% of rejection were observed. The permeate flux and rejection values obtained by GA were found to be relatively higher than that of those obtained by RSM. These results revealed that the conditions found by RSM were not assured to be optimal. Hence, GA is a powerful tool for the optimization of non-linear problems.[34-36]

3.8. Validation of the Predicted Model

In order to validate the models based on RSM-GA for separation efficiency, microfiltration experiments were carried out under optimized conditions. Permeate was collected and analysed for flux and concentration of BSA. The experiments were repeated for at least two times in order to validate the accuracy of the predicted model. The average permeate flux and rejection were found to be 4.63×10^{-5} m s^{-1} and 81.98%, respectively. These experimental results were good agreement with the results predicted by hybrid RSM-GA. In addition, the percentage deviation between the experimental and predicted results was found to be 1.278 and 0.256% for permeate flux and rejection, respectively. The permeate flux and rejection of membrane were comparable with the other reports as shown in Table 4. From the Table 4, it is clearly indicated that the fabricated zeolite membrane exhibited better separation efficiency in terms of permeate flux and rejection than the other reported literature. These results also suggested that the statistical and stochastical approaches could be effectively used to optimize the operating parameters of membrane separation operation.

4. Conclusions

MFI-type zeolite membrane was effectively fabricated on porous tubular ceramic substrate by hydrothermal synthesis technique. The fabricated membrane exhibited the porosity

of 51%, water permeability of 4.43 × 10^{-7} m^3/m^2s kPa and the average pore size of 0.272 μm. The separation efficiency of the fabricated zeolite membrane was checked with the model protein BSA in a cross-flow mode of operation. The effects of operating parameters such as BSA concentration, solution pH and applied pressure on the separation efficiency of the membrane were studied. It was experimentally demonstrated that the hybrid RSM-GA could be used to determine the parameters influencing the cross-flow microfiltration of BSA. It was observed that all the individual, interaction and quadratic terms of variables had significant influence on separation efficiency. The optimum conditions obtained using RSM-GA were validated experimentally. The separation efficiency of the membrane in terms of permeate flux and rejection were observed to be better than that of those reported in literature. The results suggest that membrane separation is cost effective and environmental compatible method for the separation of proteins. Hence, microfiltration is a promising alternate technique to the conventional separation methods of protein. Besides, this work would offer advantages in terms of the reduction in purification cost and improved recovery of BSA for the large scale operation.

Acknowledgements

We would like to thank the Central Instruments Facility at IIT Guwahati for helping us to perform FESEM analysis. The one of the author, I. Ganesh Moorthy would like to thank the Indian Academy of Sciences Bangalore, Indian National Science Academy, New Delhi and The National Academy of Sciences, Allahabad, India for the Summer Research Fellowship grant 2015.

References

1. V. Valiño, M. F. San Román, R. Ibañez and I. Ortiz, *Separation and Purification Technology*, 2014, **125**, 163-169.
2. P. Monash, A. Majhi and G. Pugazhenthi, *Journal of chemical technology and biotechnology*, 2010, **85**, 545-554.
3. J. Emilio, A. Guadix, R. Ibáñez and E. M. Guadix, *Biochemical engineering journal*, 2007, **33**, 110-115.
4. R. V. Kumar, A. K. Ghoshal and G. Pugazhenthi, *Journal of Membrane Science*, 2015, **490**, 92-102.
5. S. Khemakhem, A. Larbot and R. B. Amar, *Desalination*, 2006, **200**, 307-309.
6. S. Fakhfakh, S. Baklouti, S. Baklouti and J. Bouaziz, *Advances in Applied Ceramics*, 2010, **109**, 31-38.
7. F. Bouzerara, A. Harabi, S. Achour and A. Larbot, *Journal of the European Ceramic Society*, 2006, **26**, 1663-1671.
8. K. Khider, D. Akretche and A. Larbot, *Desalination*, 2004, **167**, 147-151.
9. G. A. Ozin, A. Kuperman and A. Stein, *Advanced Materials*, 1989, **1**, 69-86.
10. A. Persson, A.-S. Jönsson and G. Zacchi, *Journal of Membrane Science*, 2003, **223**, 11-21.
11. T. N. Shah, H. C. Foley and A. L. Zydney, *Journal of membrane science*, 2007, **295**, 40-49.
12. X. B. Ke, R. F. Shao, H. Y. Zhu, Y. Yuan, D. J. Yang, K. R. Ratinac and X. P. Gao, *Chemical Communications*, 2009, 1264-1266.
13. W. R. Bowen and D. T. Hughes, *Journal of Membrane Science*, 1990, **51**, 189-200.

14. L. Millesime, J. Dulieu and B. Chaufer, *Journal of membrane science*, 1995, **108**, 143-159.

15. P. Monash and G. Pugazhenthi, *Desalination*, 2011, **279**, 104-114.

16. X. Yi, W. Shi, S. Yu, C. Ma, N. Sun, S. Wang, L. Jin and L. Sun, *Journal of hazardous materials*, 2011, **193**, 37-44.

17. I. Xiarchos, A. Jaworska and G. Zakrzewska-Trznadel, *Journal of Membrane Science*, 2008, **321**, 222-231.

18. M. Khayet, C. Cojocaru and M. Essalhi, *Journal of Membrane Science*, 2011, **368**, 202-214.

19. K. Wegner, J. Dong and Y.S. Lin, *Journal of Membrane Science*, 1999, **158**, 17-27.

20. R.V. Kumar, A.K. Basumatary, A.K. Ghoshal and G. Pugazhenthi, *RSC Advances*, 2015, **5**, 6246-6254.

21. G. Derringer, *Journal of quality technology*, 1980, **12**, 214-219.

22. A. Konak, D. W. Coit and A. E. Smith, *Reliability Engineering & System Safety*, 2006, **91**, 992-1007.

23. C. G. Li, L. Xu, P. Wu, H. Wu and M. He, *Chemical Communications*, 2014, **50**, 15764-15767.

24. R. Szostak, *Molecular Sieve*, Blackie-Academic and Professional, 1998.

25. J. Kuhn, J. Gross, J.C. Jansen, F. Kapteijn and P.J. Jansens, *Studies in Surface Science and Catalysis*, 2007, **170**, 942-948.

26. R. H. Myers, D. C. Montgomery and C. M. Anderson-Cook, *Response surface methodology: process and product optimization using designed experiments*, John Wiley & Sons, 2009.

27. G. Box, W. G. Hunter and J. Hunter, *Statistics for experiments: an introduction to design, data analysis and modeling*,Wiley, 1978.

28. P. D. Haaland, *Experimental design in biotechnology*, CRC press, 1989.

29. S. Weisberg, *Applied linear regression*, John Wiley & Sons, 2005.

30. L. K. Cabatingan, R. C. Agapay, J. L. Rakels, M. Ottens and L. A. van der Wielen, *Industrial & engineering chemistry research*, 2001, **40**, 2302-2309.

31. C. Velasco, J. Calvo, L. Palacio, J. Carmona, P. Prádanos and A. Hernández, *Chemical Engineering Science*, 2015, **129**, 58-68.

32. M. Kosmulski, *Journal of Colloid and Interface Science*, 2009, **337**, 439-448.

33. K. Desai, S. Akolkar, Y. Badhe, S. Tambe and S. Lele, *Process Biochemistry*, 2006, **41**, 1842-1848.

34. C. C. Yuen, S. K. Gupta and A. K. Ray, *Journal of membrane science*, 2000, **176**, 177-196.

35. D. N. Mondal, K. Sarangi, F. Pettersson, P. K. Sen, H. Saxen and N. Chakraborti, *Hydrometallurgy*, 2011, **107**, 112-123.

36. R. Soleimani, N. A. Shoushtari, B. Mirza and A. Salahi, *Chemical Engineering Research and Design*, 2013, **91**, 883-903.

37. S. Fakhfakh, S. Baklouti, S. Baklouti and J. Bouaziz, *Desalination*, 2010, **262**, 188-195.

List of tables

List of figures

Table 1 Variables and its levels for RSM-FCCCD experimental design

Particulars	Variables	Levels				
		-α level	-1 level	0 level	+1 level	+α level
X_1	Concentration of BSA (ppm)	100	100	300	500	500
X_2	pH	2	2	3	4	4
X_3	Applied pressure (kPa)	68.94	68.94	172.365	275.79	275.79

Table 2 Coded and actuallevels of the independent variables according to the RSM-FCCCD experimental design and experimental results of membrane separation efficiency

	Run no	Concentration of BSA (ppm)	pH	Applied pressure (kPa)	Permeate flux (m s^{-1}) (Y_1)			Rejection (%)(Y_2)		
					Y_{exp}	Y_{pre}	Error	Y_{exp}	Y_{pre}	Error
Full factorial portion	1	100 (-1)	2 (-1)	68.94 (-1)	2.47×10^{-5}	2.48×10^{-5}	-1.1×10^{-7}	87.56	87.67	-0.1067
	2	500 (+1)	2 (-1)	68.94 (-1)	1.52×10^{-5}	1.51×10^{-5}	1.14×10^{-7}	61.68	61.69	-0.0077
	3	100 (-1)	4 (+1)	68.94 (-1)	2.69×10^{-5}	2.69×10^{-5}	4.09×10^{-9}	38.92	38.69	0.2273
	4	500 (+1)	4 (+1)	68.94 (-1)	1.67×10^{-5}	1.68×10^{-5}	-7.6×10^{-8}	42.84	43.02	-0.1787
	5	100 (-1)	2 (-1)	275.79 (+1)	4.60×10^{-5}	4.59×10^{-5}	6.41×10^{-8}	81.68	81.54	0.1433
	6	500 (+1)	2 (-1)	275.79 (+1)	4.18×10^{-5}	4.18×10^{-5}	-1.6×10^{-8}	69.98	70.24	-0.2627
	7	100 (-1)	4 (+1)	275.79 (+1)	5.54×10^{-5}	5.55×10^{-5}	-1.3×10^{-7}	48.11	48.14	-0.0277
	8	500 (+1)	4 (+1)	275.79 (+1)	5.11×10^{-5}	5.10×10^{-5}	9.41×10^{-8}	67.22	67.15	0.0713
Axial portion	9	100 (-1)	3 (0)	172.365 (0)	3.43×10^{-5}	3.41×10^{-5}	1.64×10^{-7}	63.95	64.19	-0.2362
	10	500 (+1)	3 (0)	172.365 (0)	2.69×10^{-5}	2.70×10^{-5}	-1.2×10^{-7}	61.08	60.7	0.3778
	11	300 (0)	2 (-1)	172.365 (0)	2.20×10^{-5}	2.21×10^{-5}	-5.6×10^{-8}	61.55	61.32	0.2338
	12	300 (0)	4 (+1)	172.365 (0)	2.78×10^{-5}	2.77×10^{-5}	1.04×10^{-7}	35.19	35.28	-0.0922
	13	300 (0)	3 (0)	68.94 (-1)	1.28×10^{-5}	1.27×10^{-5}	6.36×10^{-8}	52.38	52.31	0.0658
	14	300 (0)	3 (0)	275.79 (+1)	4.04×10^{-5}	4.04×10^{-5}	-1.6×10^{-8}	61.39	61.31	0.0758
Center portion	15	300 (0)	3 (0)	172.365 (0)	2.36×10^{-5}	2.36×10^{-5}	-4.9×10^{-8}	52.07	52.65	-0.5755
	16	300 (0)	3 (0)	172.365 (0)	2.38×10^{-5}	2.36×10^{-5}	1.51×10^{-7}	52.59	52.65	-0.0555
	17	300 (0)	3 (0)	172.365 (0)	2.35×10^{-5}	2.36×10^{-5}	-1.5×10^{-7}	53.04	52.65	0.3945
	18	300 (0)	3 (0)	172.365 (0)	2.37×10^{-5}	2.36×10^{-5}	5.09×10^{-8}	52.81	52.65	0.1645
	19	300 (0)	3 (0)	172.365 (0)	2.35×10^{-5}	2.36×10^{-5}	-1.5×10^{-7}	51.96	52.65	-0.6855
	20	300 (0)	3 (0)	172.365 (0)	2.37×10^{-5}	2.36×10^{-5}	5.09×10^{-8}	53.12	52.65	0.4745

Table 3 Analysis of variance of the developed second-order polynomial models for membrane separation efficiency as per the RSM-FCCD experimental design

Source	Coefficient estimate	Sum square	Degree of freedom	Mean square	*F*-value	*p*-value
Permeate flux (m s^{-1}) (Y_1)						
Model	4.46502×10^{-5}	3×10^{-9}	9	2.94×10^{-10}	15300.27	< 0.0001*
X_1	-1.31875×10^{-7}	1×10^{-10}	1	1.27×10^{-10}	6585.243	< 0.0001*
X_2	-7.51846×10^{-6}	8×10^{-11}	1	7.95×10^{-11}	4132.093	< 0.0001*
X_3	-3.5214×10^{-8}	2×10^{-9}	1	1.92×10^{-9}	99527.71	< 0.0001*
X_1X_2	-5×10^{-10}	8×10^{-14}	1	8×10^{-14}	4.156826	0.0688
X_1X_3	6.76819×10^{-11}	2×10^{-11}	1	1.57×10^{-11}	814.7378	< 0.0001*
X_2X_3	1.81291×10^{-8}	3×10^{-11}	1	2.81×10^{-11}	1461.384	< 0.0001*
X_1^2	1.73182×10^{-10}	1×10^{-10}	1	1.32×10^{-10}	6856.92	< 0.0001*
X_2^2	1.22727×10^{-6}	4×10^{-12}	1	4.14×10^{-12}	215.222	< 0.0001*
X_3^2	2.73661×10^{-10}	2×10^{-11}	1	2.36×10^{-11}	1224.421	< 0.0001*
Residual		2×10^{-13}	10	1.92×10^{-14}		
Lack of fit		1×10^{-13}	5	2.38×10^{-14}	1.62438	0.3037**
Pure error		7×10^{-14}	5	1.47×10^{-14}		
Cor total		3×10^{-9}	19			
Rejection (%)(Y_2)						
Model	144.0562	3157.829	9	350.8699	2095.651	< 0.0001*
X_1	-0.29993	30.34564	1	30.34564	181.2463	< 0.0001*
X_2	-4.7924	1694.423	1	1694.423	10120.33	< 0.0001*
X_3	-0.25702	202.5	1	202.5	1209.478	< 0.0001*
X_1X_2	0.037881	459.1965	1	459.1965	2742.657	< 0.0001*
X_1X_3	0.000177	107.8246	1	107.8246	644.0073	< 0.0001
X_2X_3	0.037648	121.2903	1	121.2903	724.4343	< 0.0001*
X_1^2	0.000245	264.0365	1	264.0365	1577.019	< 0.0001*
X_2^2	-4.34636	51.94991	1	51.94991	310.2828	< 0.0001*
X_3^2	0.00039	47.78821	1	47.78821	285.4261	< 0.0001*
Residual		1.674276	10	0.167428		
Lack of fit		0.475593	5	0.095119	0.396763	0.8334**
Pure error		1.198683	5	0.239737		
Cor total		3159.503	19			

*significant; **not significant

Table 4 Comparison of separation efficiency of zeolite membrane with other membranes

Membrane type	Pore size	Permeate flux ($m\ s^{-1}$)	Rejection (%)	Reference Number
γ-Al_2O_3 -clay composite membrane	5.4-13.6 nm	3×10^{-5}	95	2
Mixture of aluminium/titanium/zirconium oxides with an active layer of zirconium oxide	0.14 μm	4×10^{-5}	71	3
Mixed clays with titanium oxide	0.83 μm	-	40	15
Silica ceramic membrane	12.5 μm	4.31×10^{-5}	78.33	37
MFI-type zeolite membrane	0.272 μm	4.63×10^{-5}	81.98	Present work

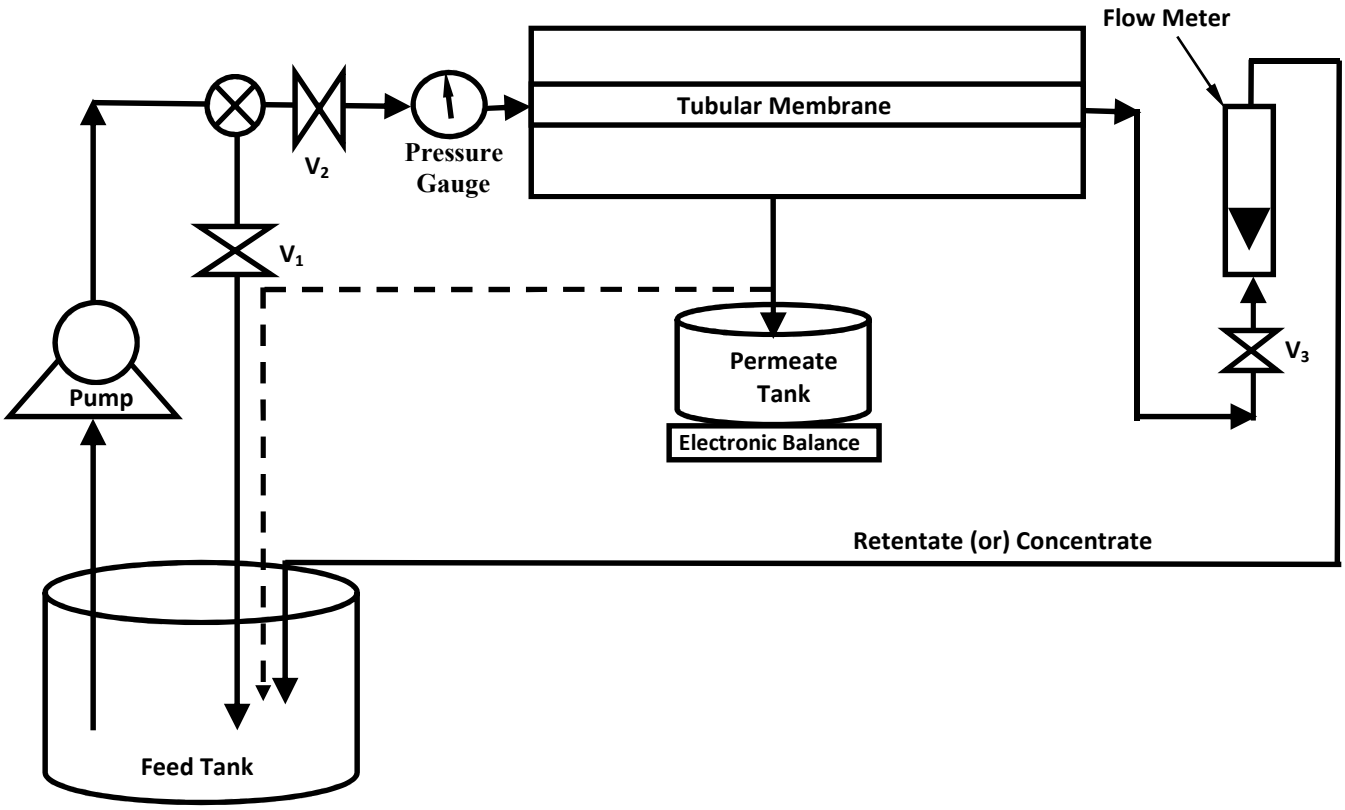

Figure 1: Schematic illustration of experimental setup of tangential system (V_1-by-pass valve, V_2- inlet valve, V_3- retentate valve)

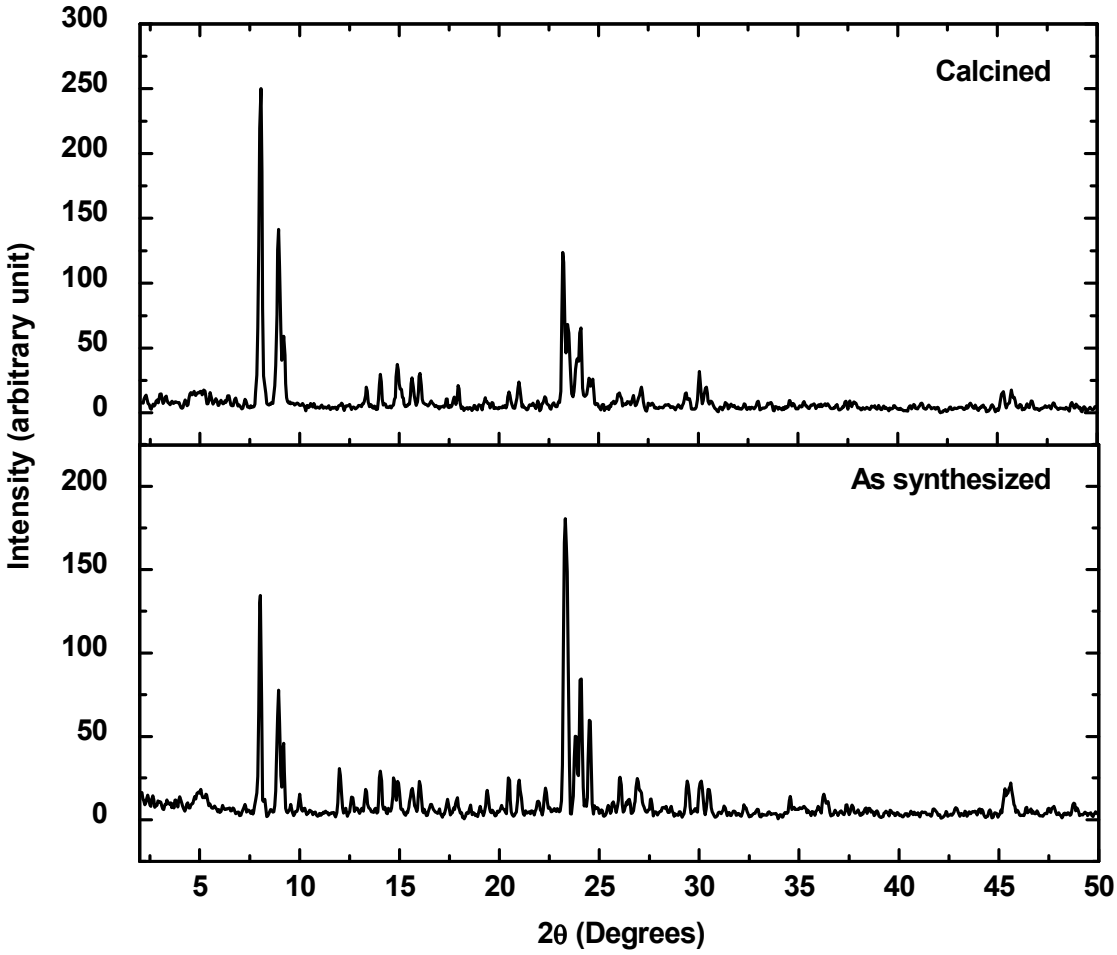

Figure 2: XRD pattern of MFI zeolite

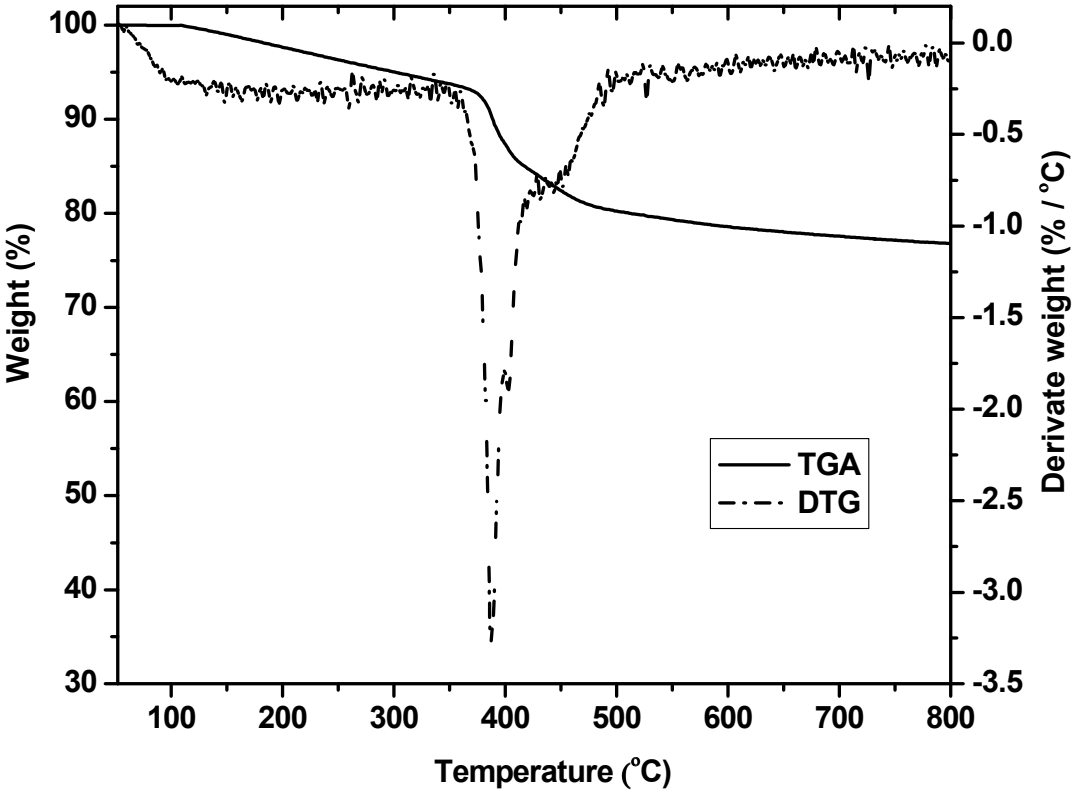

Figure 3: TGA and DTG curves of MFI zeolite

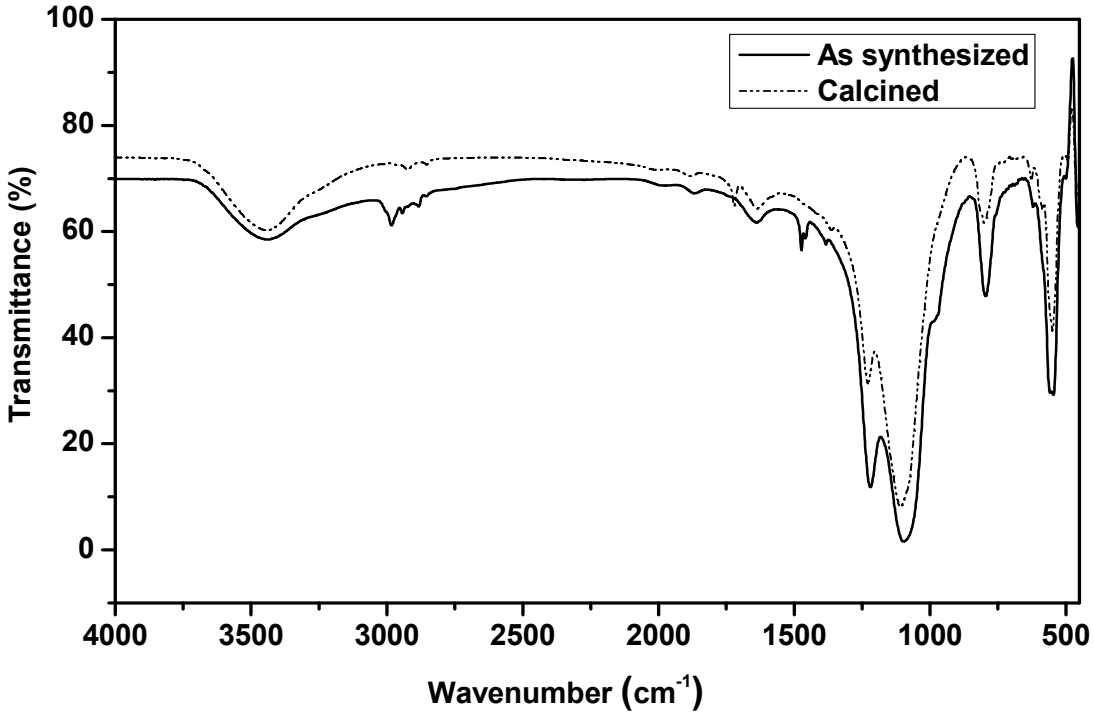

Figure 4: FTIR spectra of MFI zeolite

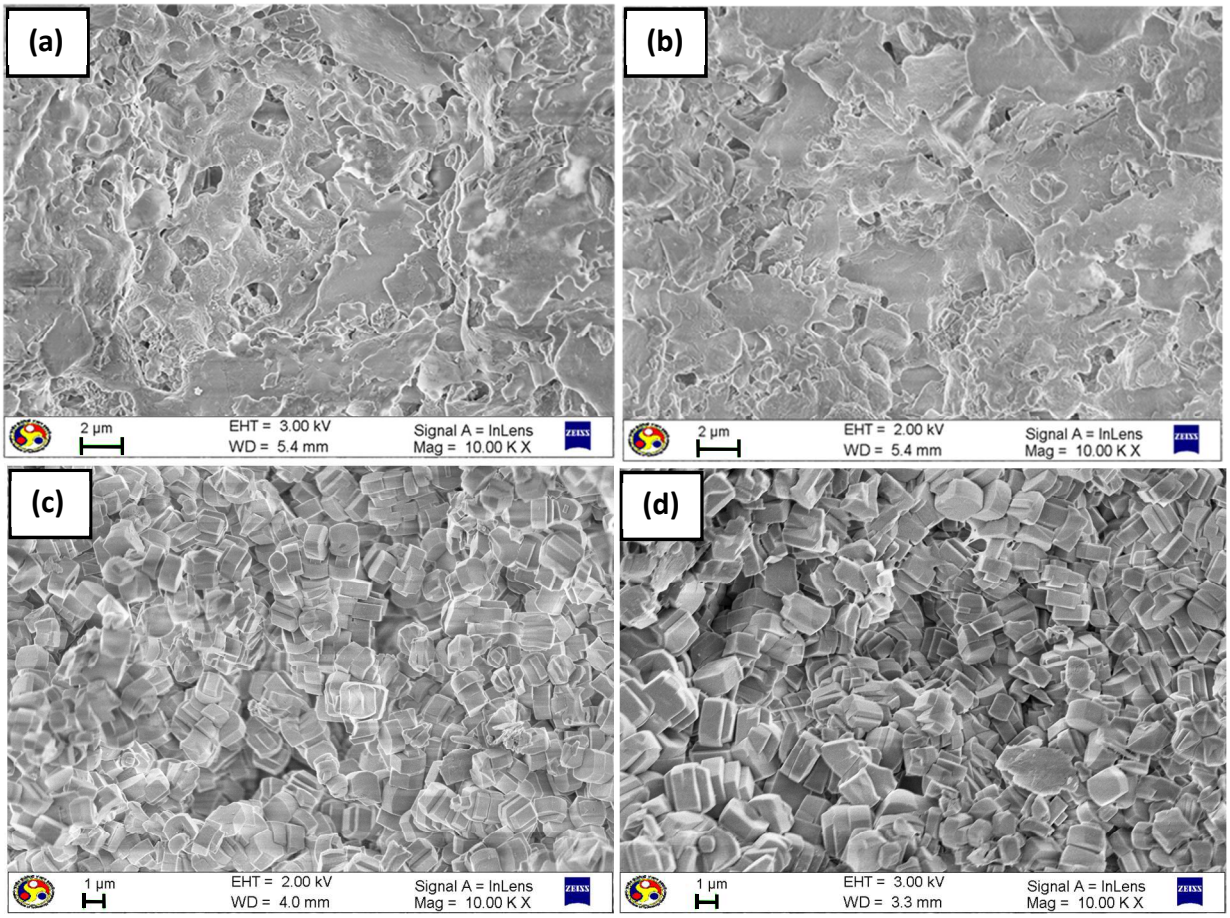

Figure 5: (a) & (b) FESEM images of inner and outer surfaces of the substrate; (c) & (d) FESEM images of inner and outer surfaces of the MFI zeolite membrane

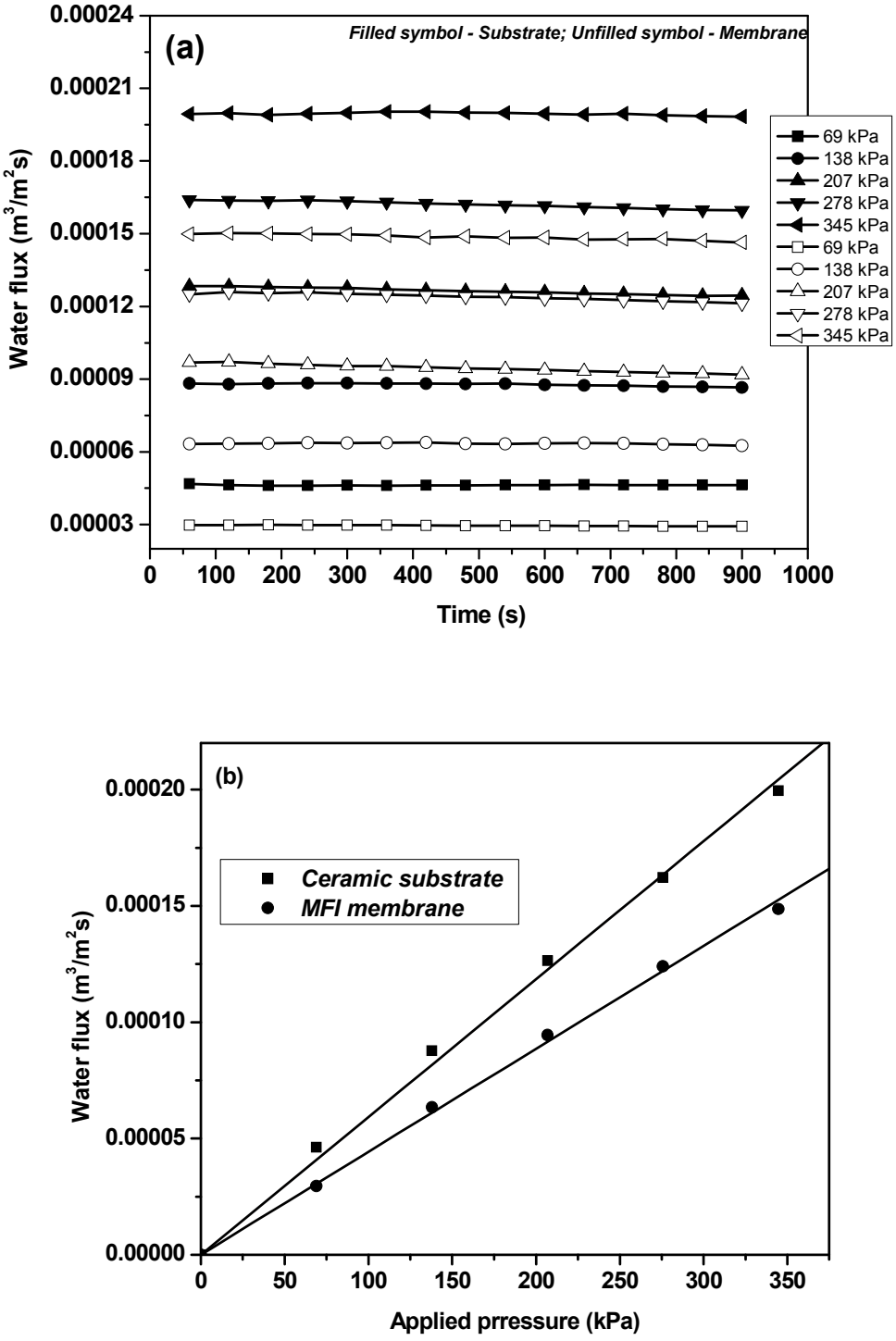

Figure 6: (a) Water flux as a function of time for five applied pressures and (b) water flux as a function of applied pressure for ceramic substrate and zeolite membrane

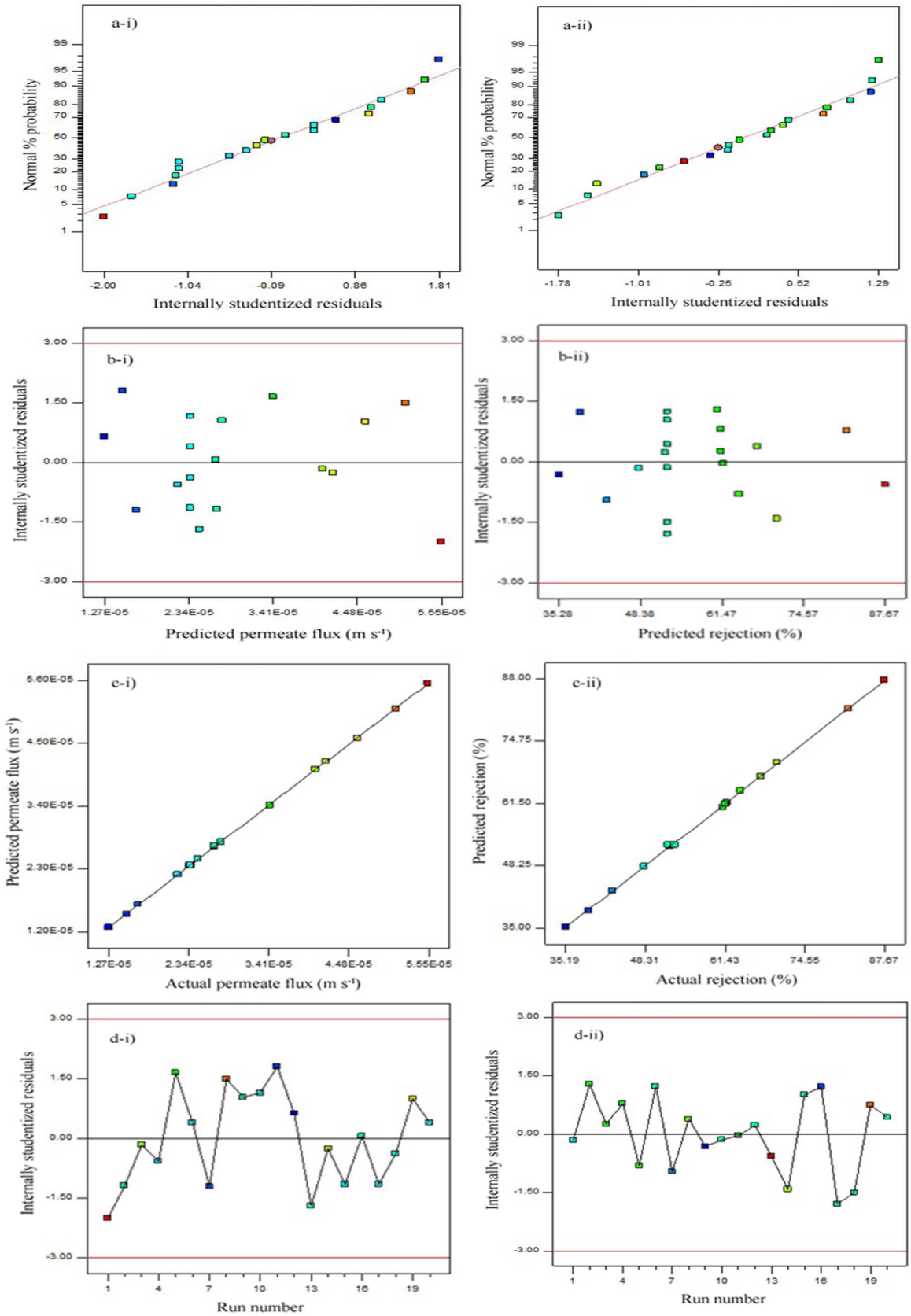

Figure 7: Diagnostic plots for the adequacy of predictive models

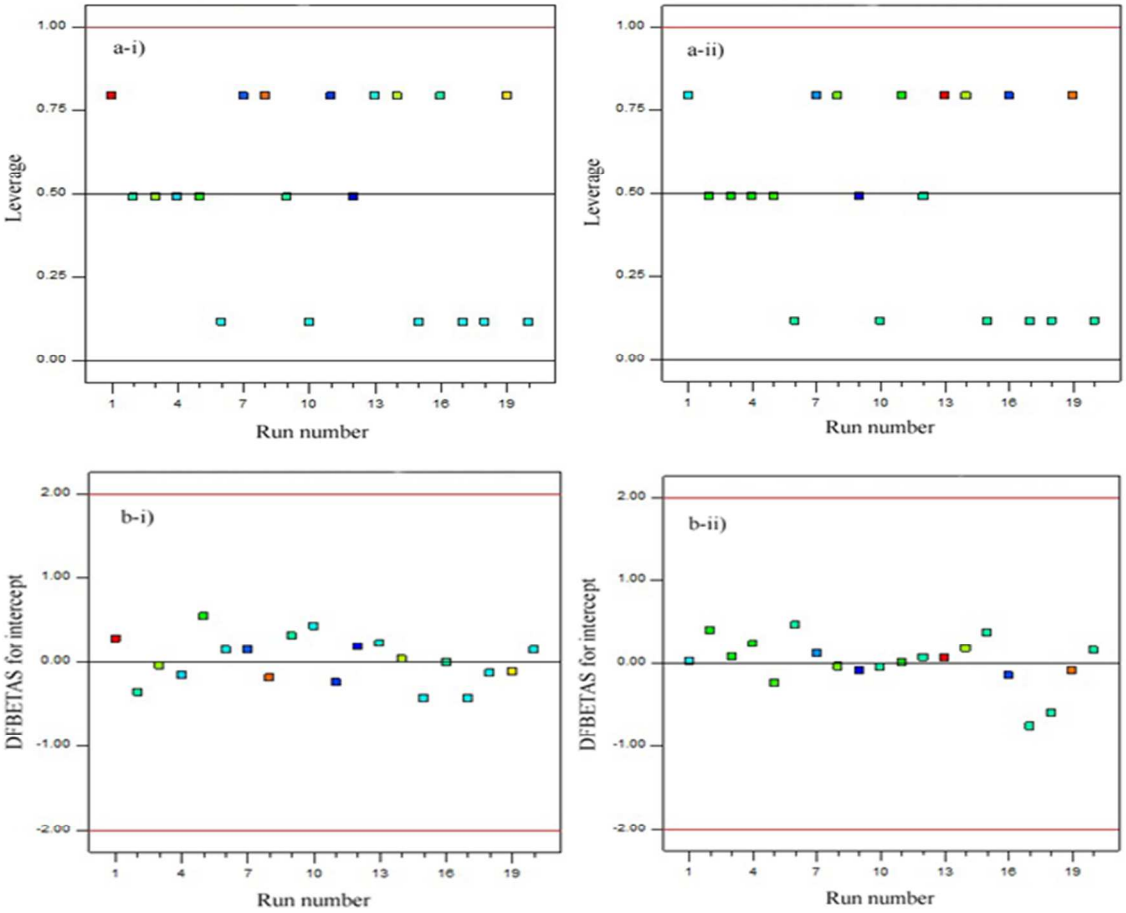

Figure 8: Influence plots for the adequacy of predictive models

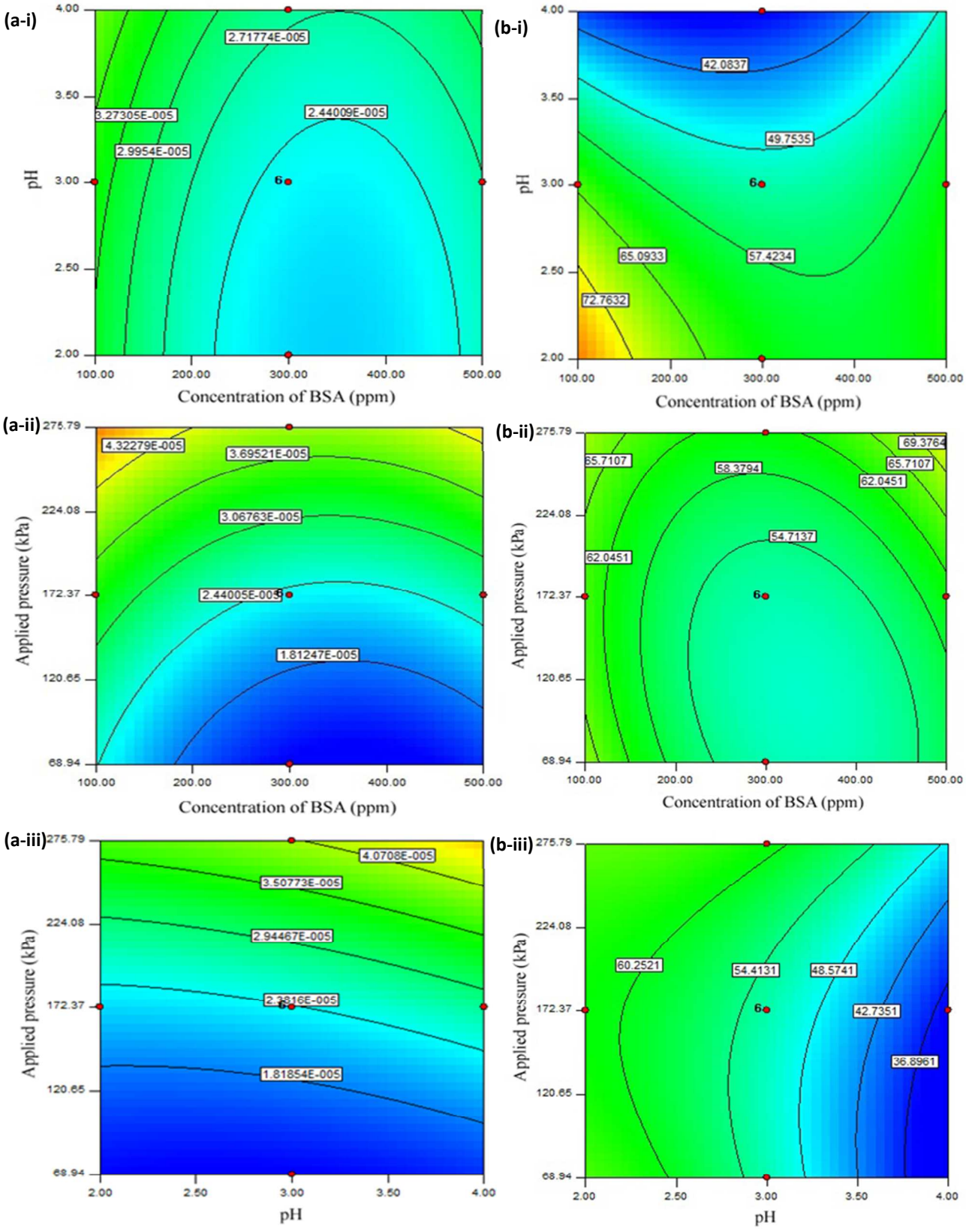

Figure 9: Contour plots representing relative effects on the responses

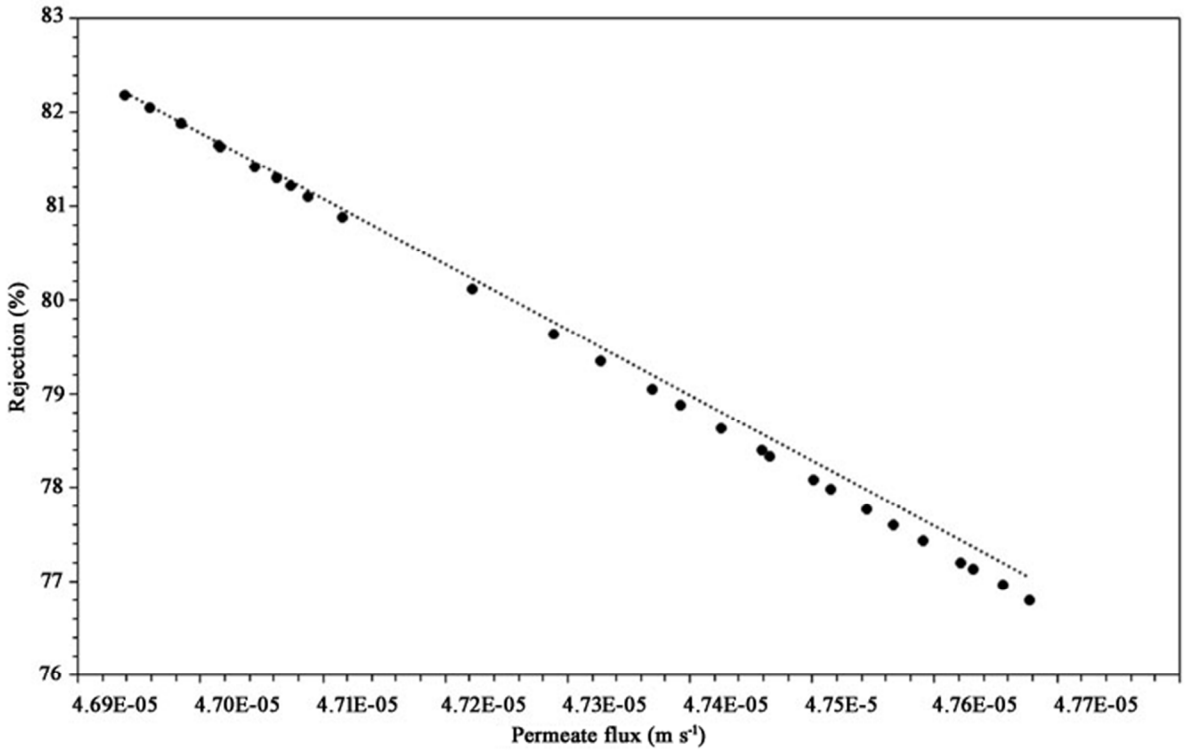

Figure 10: Pareto front plot of optimal solution set obtained from multi-response genetic algorithm technique